Magnetic Topology of Actively Evolving and Passively Convecting Structures in the Turbulent Solar Wind

B. Hnat[*] and S. C. Chapman

CFSA, Physics Department, University of Warwick, Coventry CV4 7AL, United Kingdom

N. W. Watkins

CFSA, Physics Department, University of Warwick, Coventry CV4 7AL,
United Kingdom Grantham Research Institute on Climate Change and the Environment,
LSE, London WC2A 2AE, United Kingdom and
School of Engineering and Innovation, The Open University, Milton Keynes MK7 6AA, United Kingdom

Multipoint *in situ* observations of the solar wind are used to identify the magnetic topology and current density of turbulent structures. We find that at least 35% of all structures are both actively evolving and carrying the strongest currents, actively dissipating, and heating the plasma. These structures are comprised of ~1/5 3D plasmoids, ~3/5 flux ropes, and ~1/5 3D X points consistent with magnetic reconnection. Actively evolving and passively advecting structures are both close to log-normally distributed. This provides direct evidence for the significant role of strong turbulence, evolving via magnetic shearing and reconnection, in mediating dissipation and solar wind heating.

Introduction.—Plasma turbulence and magnetic reconnection are fundamental to the transfer of energy and momentum between field and flow and are ubiquitous, from the explosive confinement collapse in laboratory plasmas [1], to stellar flares [2], solar wind acceleration [3] and its interaction with planetary magnetospheres [4], and magnetic field generation in newly formed galaxy clusters [5]. *In situ* spacecraft observations of the solar wind have provided indirect, but consistent, evidence that energy is transported nonlinearly across multiple scales and between different classes of fluctuations [6]. While it is well established that energy can reach the ion gyro scale via a magnetohydrodynamic (MHD) turbulent energy cascade [7], how this is channeled to the electron dissipation scale remains an open question [8]. There is growing evidence that magnetic reconnection may be an essential component of solar wind evolution [9], converting magnetic field energy into heat and kinetic energy via a topological change to the magnetic field. Both processes generate coherent structures, and both can, in principle, occur in the high Mach number solar wind. Elucidating the topological features of these structures and quantifying what fraction is actively evolving has the potential to explain their role in particle acceleration and collisionless plasma heating, which are both outstanding questions for plasma physics. The methodology used in this Letter builds on extensive application in hydrodynamic (HD) turbulence, where it provided clear evidence for sheetlike structures dominating dissipation scale dynamics [10]. Multipoint satellite observations offer a unique opportunity to directly probe the properties of the coherent structures inherent in plasma turbulence and reconnection.

Long-lived, coherent structures are ubiquitous in both laboratory and astrophysical plasmas [11]. In the solar wind, the magnetic field can form tangential or rotational discontinuities [12], current sheets [13,14] and neutral X lines [15]. Tangential discontinuities arise at the interfaces of magnetic flux tubes [16], while current sheets may be generated by straining plasma motions [17,18]. Some of these structures could also be of solar origin, passively advected by the solar wind [19]. Recent work identified predominantly elliptic magnetic topology with a gradual transition from quasi-2D to 3D structures for a decreasing spatial scale [20]. Magnetic structures contribute significantly to the observed scale-free power spectrum of magnetic fluctuations in the solar wind at MHD scales [16,21]. Current driven structures have been statistically associated with Ohmic electron heating [22] and events characterized by large intermittent currents are routinely used as proxies of dissipation [23]. Thin current sheets in the turbulent medium are unstable to tearing instability, modifying the energy transfer rates between fields and plasma on different scales [24]. The contribution of magnetic null structures to plasma heating has not been directly quantified. Analytical studies of MHD systems have established that the magnetic nulls are preferential sites for the formation of large coherent structures [18], independent of the initial conditions. It has also been shown [2] that in MHD scalar pressure equilibria, the stable null points must have 3D X-point topology.

However, not all current carrying structures are actively evolving and participating in Ohmic heating. Current carrying, force-free magnetic field configurations (FFMFC) are energy minimizing states for a given magnetic helicity and are stable on long timescales. Conversely, magnetic field X points with small current density may become unstable to tearing mode instability and grow significant currents [13]. In this Letter, we discriminate quantitatively between structures that are actively evolving and those that are passively advecting in the solar wind. We show that quasi-2D magnetic flux rope topology is most likely to have large currents and to actively evolve in the solar wind, while multipole neutral X-point structures may evolve, but carry small currents. About 25% of all structures are FFMFC and hence passively advecting. These findings support the coexistence of reconnection and turbulence in the solar wind, and their importance in solar wind heating.

Data and methods.—We analyze six intervals (Table I) of solar wind magnetic field measured by Cluster FGM [25]. The Cluster tetrahedron was in a pseudo-sphere configuration with elongation and coplanarity both below 0.4. The characteristic length scale of the formation $D_{sc} \approx 210$ km for intervals 1–5, spanning 2–4 proton Larmor radii ρ_p. Interval 6, used to validate the MHD assumptions, has plasma parameters similar to those of intervals 1–5 but $D_{sc} \approx 3600 \approx 35\rho_p$, which is in the MHD regime. All intervals have proton plasma $\beta_p < 1$. Figures 1(a),1(b) plot the plasma parameters and magnetic field for interval 3 of Table I. Particle spectra from the CIS [26] and PEACE [27] instruments, not shown, confirm that no intervals were contaminated by the foreshock.

Cluster FGM samples at $f_s \approx 22$ Hz, giving 3.2×10^5 samples for intervals 1–5. To construct the magnetic field gradient tensor at this cadence, we interpolate magnetic field and spacecraft position from the time grid of C2, C3, and C4 spacecraft onto the time base of spacecraft C1, for each interval. We then construct at each time a coarse-grained magnetic field gradient tensor (MFGT) averaged over the volume V enclosed by the multispacecraft tetrahedron:

$$A_{ij} = \frac{1}{V} \int_V \frac{\partial B_i}{\partial r_j} d^3 r. \quad (1)$$

TABLE I. Summary of investigated Cluster intervals.

Interval date and time	β_p	ρ_p (d_i) [km]
1. 27-Jan-04 00:36-01:18	0.44	63.2 (77.5)
2. 31-Jan-04 14:30-14:55	0.75	137.1 (124.8)
3. 21-Feb-04 17:25-18:45	0.62	72.9 (72.9)
4. 22-Feb-04 03:15-04:10	0.66	66.1 (64.1)
5. 29-Feb-04 04:10-04:50	0.84	157.9 (135.7)
6. 10-Feb-03 18:15-19:45	0.97	107.6 (43.2)

The MFGT A is constructed from data using relative position vectors ρ_i and the magnetic field differences b_i, $i = 1, 2, 3$, between spacecraft [28]. Defined with respect to the center of the volume V, $\rho_1 = (R_1 - R_2)/\sqrt{2}$, $\rho_2 = (R_1 + R_2 - 2R_3)/\sqrt{6}$, and $\rho_3 = (R_1 + R_2 + R_3 - 3R_4)/\sqrt{12}$, and R_s is a position vector of spacecraft s in GSE coordinates. Similarly, $b_1 = (B_1 - B_2)/\sqrt{2}$, $b_2 = (B_1 + B_2 - 2B_3)/\sqrt{6}$, and $b_3 = (B_1 + B_2 + B_3 - 3B_4)/\sqrt{12}$, B_s is the magnetic field vector at spacecraft s. Inverting the relation $\mathbf{b} = A\rho$ with the constraint $\nabla \cdot \mathbf{b} = 0$ gives the tensor elements $A_{ij} = (b\rho^{-1})_{ij} - \delta_{ij} \text{tr}(b\rho^{-1})/3$. The error, $|\nabla \cdot \mathbf{B}|/|\nabla \times \mathbf{B}|$ [29], from neglecting higher order terms in this approximation never exceeds 3% here.

Structures topology and evolution.—The classification of magnetic field line topology is identical to that of trajectories near critical points in dynamical systems [30]. The tensor principal invariants [31] are independent of a coordinate system and are the coefficients of the characteristic equation $|A - \lambda_i I| = \lambda_i^3 + P\lambda_i^2 + Q\lambda_i + R = 0$, where $\lambda_i \in \mathbb{C}$ are the eigenvalues of A. These invariants can be expressed using

$$P = -\text{tr}(A) = 0, \qquad Q = -\frac{1}{2}\text{tr}(A^2), \qquad R = -\frac{1}{3}\text{tr}(A^3). \quad (2)$$

The sign of the determinant of the characteristic equation $D = 27/4R^2 + Q^3$ defines two regions in the (R,Q) plane. When $D > 0$, two eigenvalues of A are complex and one is real, while for $D < 0$ all three eigenvalues are real. The sign of R discriminates between two different polarities (directions) of the magnetic field for each topology. Structures with $D > 0$ generalize a 2D O point in three dimensions,
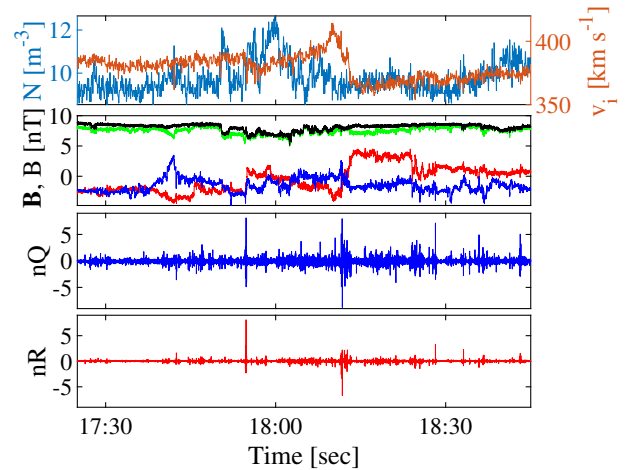
FIG. 1. Solar wind magnetic field and bulk flow parameters observed by Cluster on 21-Feb-2004: (a) ion number density n_i (blue) and solar wind ion bulk speed v_i (red); (b) magnetic field vector components in GSE coordinates (B_x-red, B_y-green, B_z-blue) and magnitude (black). (c),(d) Normalized invariants nQ and nR of the magnetic field gradient tensor.

while topologies with $D < 0$ are the 3D generalization of a 2D X point. We employ a simplified terminology for these topologies, and refer the reader to Fig. 8(b) of Ref. [32] for a detailed classification. Invariants with $D > 0$ indicate elliptic magnetic field lines, which form 3D plasmoids ($|R| \gg 0$), or quasi-2D flux ropes ($R \sim 0$). Here, plasmoids are finite length, self-contained structures, while quasi-2D flux ropes have a negligible magnetic field variation along the structure, on the scale of the tetrahedron. For $D < 0$ the field lines are hyperbolic, forming multipole separatrix structures consistent with 3D reconnection (3D X points). The relative prevalence of magnetic X points quantifies the potential impact of reconnection on turbulent energy transfer via current sheet disruption, which can translate to plasma heating. These hyperbolic structures are fully three-dimensional and can have a strong guide field with signatures [24] that do not trivially map onto reconnection sites identified via the classic quasi-2D picture of shear reversal and outflow [33]. Additional information can be inferred from the antisymmetric part of A. The current density rate tensor J relates magnetic field lines and current, $j_k = \epsilon_{ijk} J_{ij}$ via the Faraday law $\nabla \times B = \mu_0 j$. An additional invariant related to J is defined such that $2Q_j = -\text{tr}(J^2)$. Thus, Q_j is directly related to the current density magnitude $|j|$, since $4Q_j = j^2$.

As well as classifying the topology of fluctuations by their values of $D(Q, R)$, we can establish whether they are actively evolving by determining if their magnetic configuration is close to that of an FFMFC. An approximate condition for force-free fields is that the current is locally parallel to the magnetic field, i.e., $|\zeta| \sim 1$, where

$$\zeta = \cos \alpha = (\nabla \times \langle B \rangle_s) \cdot \langle B \rangle_s / (|\nabla \times \langle B \rangle_s| \langle B \rangle_s), \quad (3)$$

and $\langle B \rangle_s$ is the average magnetic field of all four Cluster spacecraft. Equation (3) neglects the possible impact of thermal pressure on the evolution of the magnetic structures [34]. Since the CIS instruments operate only on two spacecraft we cannot construct ∇p for direct comparison with $j \times B$. However, gradients are observed on the same spatial scale for all quantities; direct comparison between thermal and magnetic pressure confirms that $\sim 80\%$ of all FFMFC (intervals 1–6) occurred when $p_{\text{th}} < p_B$, supporting the approximation underlying (3).

Results.—We constructed the tensor A and its invariants from each temporal measurement of four magnetic field vectors sampled by the Cluster in each interval 1–5. The invariants are normalised by the power in j^2 in each interval, and these normalized quantities are analyzed below. Panels (c),(d) of Fig. 1 plot the time series of $nQ(t) = Q(t)/\langle j^2 \rangle$ and $nR(t) = R(t)/\langle j^2 \rangle^{3/2}$ for the selected interval. We have verified the approximately scale-free power spectra of the magnetic field, non-Gaussian
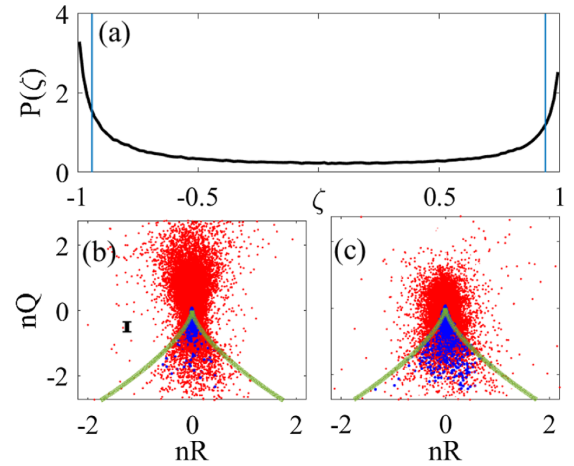
FIG. 2. (a) Probability density of counts $P(\zeta)$, combined for intervals 1–5. Blue vertical lines indicate the limits of passive (active) magnetic field configurations. (b),(c) Scatter plots of (nR, nQ) pairs combined for intervals 1–5: (b) a FFMFC, $|\zeta| > 0.94$ and (c) magnetic field departing from FFMFC, $|\zeta| < 0.94$. The points are colored according to the current density magnitude: red —$|j| > \sigma_j$, blue (plotted over the red)—$|j| < \sigma_j$, where σ_j is a standard deviation of $|j|$. Solid green line shows the curve of $D = 0$. Black cross in panel (b) indicates the error estimated from the magnetometer uncertainty of 0.1 nT.

distribution of the MFGT elements and high intermittency of the invariants, confirming that the magnetic field is turbulent.

The probability density $P(\zeta)$ for the combined intervals 1–5, shown in Fig. 2(a) identifies $\sim 25\%$ of all structures as being passively advecting with FFMFC satisfying $\zeta > 0.94$ using Eq. (3), that is, the angle $\alpha < 20°$. We verified that our results are not strongly dependent on this threshold until $\alpha > 30°$. The magnetic field topology of each structure can be classified by its location in the nQ, nR plane. Figure 2(b) is a combined scatter plot of the invariants $nQ(t)$, $nR(t)$ of the passively advecting population in intervals 1–5. The black error bar indicates the typical nQ and nR uncertainty obtained by propagating magnetic field component uncertainty 0.1 nT and assuming no uncertainty in the spacecraft position. The 75% of the combined population that are unambiguously not force-free, those with $|\zeta| < 0.94$, are plotted in panel (c). The solid green line is the separatrix, $D = 0$ and summing counts of observed structures above and below this line indicates that the 25% of the total that are passively advecting structures, are themselves comprised of 3D plasmoids ($D > 0$, $|nR| > 0.05$), quasi-2D flux ropes ($D > 0$, $|nR| < 0.05$), and 3D neutral line X-point ($D < 0$) topologies, in the ratio 0.19 : 0.54 : 0.27. In contrast, the actively evolving population is in the ratio 0.09 : 0.52 : 0.39, dominated by quasi-2D flux ropes and 3D X points. In panels (b),(c), points are colored indicating the magnitude of the current density $|j| = \sqrt{j^2}$, calculated from the invariant Q_j: red indicates intense currents,
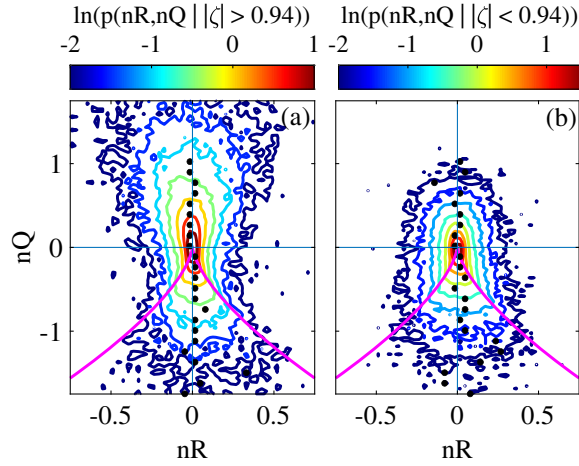
FIG. 3. Conditional joint probability density for combined intervals 1–5: (a) $p(nR, nQ||\zeta| > 0.94)$; (b) $p(nR, nQ||\zeta| < 0.94)$. Solid magenta line indicates $D = 0$ curve.

FIG. 4. Combined probability density $P(j^*||\zeta| > 0.94)$ (red squares) and $P(j^*||\zeta| < 0.94)$ (blue squares), where the current is standardized $j* = (|j| - \langle|j|\rangle)/\sigma_{|j|}$. Black lines plot a normal distribution for the logarithm of $P(j^*)$ with zero mean and unit standard deviation.

$|j| > \sigma_j$, blue corresponds to small currents, $|j| < \sigma_j$, where σ_j is a standard deviation of $|j|$. Generally, plasmoid or flux rope topologies are associated with intense currents whereas 3D neutral line topology is associated with weak currents. A zero current at the neutral line necessarily requires a symmetric tensor with three real eigenvalues. However, the converse is not true, that is, finding an X-point null topology does not necessarily indicate a lack of current. At least 2/3 of all large current configurations are plasmoid or flux rope type, while only 1/5 of large currents are associated with neutral line structures. These proportions are approximately the same across all structures whether force-free or not.

The above characterization places a lower bound on the fraction of structures that are both actively evolving and have large currents, which we find is ∼35% of the total population. They are in the ratio 0.18:0.6:0.22 for 3D plasmoids, flux ropes, and 3D X points. These structures can actively evolve, modifying the turbulent transfer rates of energy which ultimately dissipates, hence heating the solar wind. In order to assess the statistical significance of the topological structures in the scatter plots of Fig. 2, we construct the joint conditional probability density functions (pdf) for the passive structures with FFMFC $p(nR, nQ||\zeta| > 0.94)$, and for the evolving structures $p(nR, nQ||\zeta| < 0.94)$. Figures 3(a),3(b) show contours of the logarithms of these pdfs. Solid black circles indicate the positions of maxima in p for a subset of nQ values. The contour with the lowest probability density corresponds to 10 samples per bin. These distributions confirm our previous findings: the passive structures consist mostly of 3D plasmoids and quasi-2D flux tubes while actively evolving magnetic configurations are quasi-2D flux tubes and 3D X points. The maxima of combined distributions in Figs. 3(a),3(b) are nearly symmetric with respect to the $nR = 0$ line, and only the three central contours in
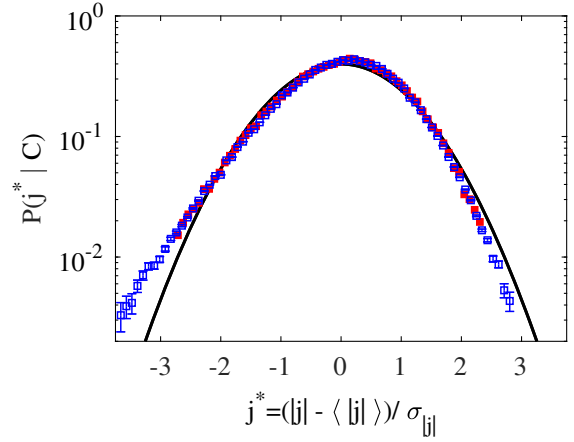
panel (b) show a preference for the $nR > 0, D < 0$ quadrant.

Having established the dominant topology of the passive and actively evolving magnetic field structures, we examine the statistics of their current densities. Figure 4 shows the pdfs $P(j^*)$, on semilog axes, of the standardized current density $j^* = (|j| - \langle|j|\rangle)/\sigma_{|j|}$ for passive (red squares) and active (blue squares) structures. Black lines represent a normal distribution of $\log(P^*)$ with zero mean and unit standard deviation. Clearly, the functional forms of the distribution of current density associated with both the passively advecting and actively evolving structures are essentially the same. Thus, evolving and passively advecting structures cannot be discriminated solely by the functional form of their pdf. They are both close to, but slightly skewed compared to a log-normal pdf. The fact that the pdf form does not discriminate between passive and active structures highlights the need to go beyond statistical characterization to determine the relative importance of turbulent processes for solar wind evolution and heating.

Conclusions.—There is mounting evidence that the coexistence of turbulence and magnetic reconnection in the solar wind modifies the balance of energy transfer between different scales [6]. The precise energy balance depends on the relative prevalence of specific topological structures present in the plasma, their rate of evolution and their ability to carry currents. We classified the magnetic field topology to quantitatively estimate the prevalence of actively evolving and passively advective structures and their contribution to Ohmic heating. We established that at least 25% of all samples have the FFMFC, passively advected by the solar wind. The passive structures are dominated by elliptic field lines (plasmoids) which carry a significant current density. Magnetic structures that are

actively evolving are primarily quasi-2D flux ropes and 3D X points. Magnetic configurations that actively evolve and carry a significant current, give a lower bound on the fraction of structures that can dissipate and heat the plasma to be $\sim$35% of the total population. These are dominated by quasi-2D flux rope topology. Magnetic X-point topology comprises $\sim$40% of all evolving structures, but only 1/5 of these hyperbolic 3D X points carry a significant current. Criteria for plasma heating that set a lower threshold on the current are likely to significantly underestimate the importance of reconnection. Our results are in agreement with recent analysis of magnetic field topology in the solar wind [20] and with results from direct MHD numerical simulations [35], which, unlike HD [10] also show no R asymmetry. These MHD studies did not test whether the structures were actively evolving or were force-free. Identifying a significant FFMFC population informs development of solar wind turbulence models which include small scale reconnection but assume that all structures are actively evolving [24].

The preferential association of flux ropes and plasmoids with large currents is consistent with a reconnection rate proportional to the current. The timescale of dynamical evolution of structures with stronger currents would be fast; their observations dominated by pre- and postreconnection states. Evolving X points with negligible currents would be tearing unstable, rapidly generating 3D plasmoids with significant current levels [13]. The scale of the Cluster formation may be too large to reliably detect the full effect of reconnection using the MFGT [36]. Nevertheless, we quantify the contribution of these magnetic field structures to the dynamical evolution of the plasma, offering new insight into the role of turbulence and reconnection in active plasma mixing and thermalization.

---

[*]B.Hnat@warwick.ac.uk

[1] B. B. Kadomtsev, Plasma Phys. Control. Fusion **26**, 217 (1984).

[2] Y. T. Lau and J. M. Finn, Astrophys. J. **350**, 672 (1990).

[3] S. R. Cranmer, A. A. Van Ballegooijen, and R. J. Edgar, Astrophys. J. Suppl. Ser. **171**, 520 (2007).

[4] G. Paschmann, B. U. Ö. Sonnerup, I. Papamastorakis, N. Sckopke, G. Haerendel, S. J. Bame, J. R. Asbridge, J. T. Gosling, C. T. Russell, and R. C. Elphic, Nature (London) **282**, 243 (1979).

[5] K. Subramanian, A. Shukurov, and N. E. L. Haugen, Mon. Not. R. Astron. Soc. **366**, 1437 (2006).

[6] W. H. Matthaeus and M. Velli, Space Sci. Rev. **160**, 145 (2011).

[7] C. W. Smith, W. H. Matthaeus, G. P. Zank, N. F. Ness, S. Oughton, and J. D. Richardson, J. Geophys. Res. **106**, 8253 (2001); B. J. Vasquez et al., J. Geophys. Res. **112**, A07101 (2007); J. T. Coburn, C. W. Smith, B. J. Vasquez, J. E. Stawarz, and M. A. Forman, Astrophys. J. **754**, 93 (2012).

[8] O. Alexandrova, V. Carbone, P. Veltri, and L. Sorriso-Valvo, Astrophys. J. **674**, 1153 (2008); K. H. Kiyani, S. C. Chapman, Y. V. Khotyaintsev, M. W. Dunlop, and F. Sahraoui, Phys. Rev. Lett. **103**, 075006 (2009).

[9] J. T. Gosling, Space Sci. Rev. **172**, 187 (2012); K. T. Osman, W. H. Matthaeus, J. T. Gosling, A. Greco, S. Servidio, B. Hnat, S. C. Chapman, and T. D. Phan, Phys. Rev. Lett. **112**, 215002 (2014).

[10] P. Vieillefosse, Physica (Amsterdam) **125A**, 150 (1984); B. J. Cantwell, Phys. Fluids A **5**, 2008 (1993); N. E. Sujovolsky and P. D. Mininni, Phys. Rev. Fluids **5**, 064802 (2020); S. Suman and S. S. Girimaji, Phys. Fluids **25**, 125103 (2013).

[11] M. Yamada, R. Kulsrud, and H. Ji, Rev. Mod. Phys. **82**, 603 (2010).

[12] L. F. Burlaga, J. Geophys. Res. **76**, 4360 (1971).

[13] D. Biskamp, *Nonlinear Magnetohydrodynamics* (Cambridge University Press, Cambridge, England, 2009), Vol. 1.

[14] S. Perri, M. L. Goldstein, J. C. Dorelli, and F. Sahraoui, Phys. Rev. Lett. **109**, 191101 (2012).

[15] T. D. Phan et al., Nature (London) **557**, 202 (2018); M. S. Davis, T. D. Phan, J. T. Gosling, and R. M. Skoug, Geophys. Res. Lett. **33**, L19102 (2006).

[16] J. E. Borovsky, Phys. Rev. Lett. **105**, 111102 (2010).

[17] W. H. Matthaeus and D. Montgomery, Ann. N.Y. Acad. Sci. **357**, 203 (1980).

[18] V. Carbone, P. Veltri, and A. Mangeney, Phys. Fluids **2**, 1487 (1990).

[19] C.-Y. Tu and E. Marsch, J. Geophys. Res. **99**, 21481 (1994).

[20] V. Quattrociocchi, G. Consolini, M. F. Marcucci, and M. Materassi, Astrophys. J. **878**, 124 (2019).

[21] S. Lion, O. Alexandrova, and A. Zaslavsky, Astrophys. J. **824**, 47 (2016).

[22] J. L. Burch et al., Science **352**, aaf2939 (2016).

[23] K. T. Osman, W. H. Matthaeus, A. Greco, and S. Servidio, Astrophys. J. Lett. **727**, L11 (2011); M. Wan, W. H. Matthaeus, H. Karimabadi, V. Roytershteyn, M. Shay, P. Wu, W. Daughton, B. Loring, and S. C. Chapman, Phys. Rev. Lett. **109**, 195001 (2012).

[24] S. Boldyrev and N. F. Loureiro, Astrophys. J. **844**, 125 (2017); D. Vech, A. Mallet, K. G. Klein, and J. C. Kasper, Astrophys. J. Lett. **855**, L27 (2018).

[25] A. Balogh et al., Space Sci. Rev. **79**, 65 (1997).

[26] H. Rème et al., Ann. Geophys. **19**, 1303 (2001).

[27] A. D. Johnstone et al., PEACE: A plasma electron and current experiment, *The Cluster and Phoenix Missions* (Springer, Dordrecht, 1997), pp. 351–398.

[28] M. Chertkov, A. Pumir, and B. I. Shraiman, Phys. Fluids **11**, 2394 (1999).

[29] Analysis methods for multi-spacecraft data, edited by G. Paschmann and P. W. Daly ISSI Scientific Report No. SR-001, 1998.

[30] P. J. Morrison, Phys. Plasmas **7**, 2279 (2000).

[31] B. J. Cantwell, Phys. Fluids A **4**, 782 (1992); C. Meneveau, Annu. Rev. Fluid Mech. **43**, 219 (2011).

[32] M. S. Chong, A. E. Perry, and B. J. Cantwell, Phys. Fluids **2**, 765 (1990).

[33] J. T. Gosling, J. Geophys. Res. **110**, A1 (2005).

[34] D. B. Reisenfeld, D. J. McComas, and J. T. Steinberg, Geophys. Res. Lett. **26**, 1805 (1999); P. J. Kellogg and T. S. Horbury, Ann. Geophys. **23**, 3765 (2005).

[35] V. Dallas and A. Alexakis, Phys. Fluids **25**, 105106 (2013).

[36] M. Wan, W. H. Matthaeus, S. Servidio, and S. Oughton, Phys. Plasmas **20**, 042307 (2013).